We are IntechOpen, the world's leading publisher of Open Access books Built by scientists, for scientists

4,800
Open access books available

122,000
International authors and editors

135M
Downloads

Our authors are among the

154
Countries delivered to

TOP 1%
most cited scientists

12.2%
Contributors from top 500 universities

CLARIVATE ANALYTICS
BOOK CITATION INDEX
INDEXED

WEB OF SCIENCE™

Selection of our books indexed in the Book Citation Index
in Web of Science™ Core Collection (BKCI)

Interested in publishing with us?
Contact book.department@intechopen.com

Numbers displayed above are based on latest data collected.
For more information visit www.intechopen.com

Chapter

NFC Sensors Based on Energy Harvesting for IoT Applications

Antonio Lazaro, Marti Boada, Ramon Villarino and David Girbau

Abstract

The availability of low-cost near-field communication (NFC) devices, the incorporation of NFC readers into most current mobile phones, and the inclusion of energy-harvesting (EH) capabilities in NFC chips make NFC a key technology for the development of green Internet of Things (IoT) applications. In this chapter, an overview of recent advances in the field of battery-less NFC sensors at 13.56 MHz is provided, and a comparison to other short-range RFID technologies is given. After reviewing power transfer in NFC, recommendations for the practical design of NFC-based sensor tags and NFC readers are made. A list of commercial NFC integrated circuits with energy-harvesting capabilities is also provided. A survey of recent battery-less NFC sensors developed by the group including soil moisture, water content, pH, color, and implanted NFC sensors is done.

Keywords: battery-less, near-field communication (NFC), radiofrequency identification (RFID), energy harvesting, implantable medical devices, wireless power transfer (WPT), internet of things (IoT)

1. Introduction

In recent years, radio identification (RFID) technology [1, 2] has grown extraordinarily. Initially, it came to replace barcodes for product identification [3]. Nowadays, there are several frequency bands and a number of applications [2]. RIFD can be classified depending on the frequency band used: low frequency (LF), high frequency (HF), ultrahigh frequency (UHF), or microwave bands [2]. Another classification refers to the power source: tags can be passive if they harvest the energy from the RF interrogating signal of the reader or active if the energy to feed the electronics is obtained from a battery. The communication in passive tags is based on backscattering communication and consists on modulating the load that modifies the radar cross section of the antenna [4, 5]. Although UHF readers are expensive (1–2 k$), the inlays designed for traceability are cheap, and the return on investment (ROI) is possible due to the large number of units involved. The read range can be increased by improving the IC sensitivity (e.g., −22 dBm for Impinj Monza R6) allowing to reach several meters (about 10–15 m). There exist also semi-passive or battery-assisted tags (BAP) that use battery to feed only the electronics needed to improve the sensitivity, but the communication is based on backscattering as in the passive tags [6–8]. The cost of UHF BAP tags is often lower than active
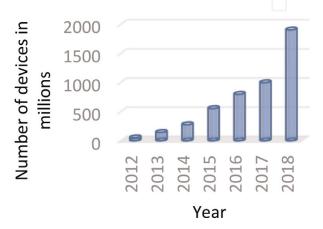
tags based on transceivers such as Bluetooth low energy (BLE), Zigbee, etc. Recently, several UHF BAP transponders have appeared in the market such as the AMS-SL900A IC [7, 9]. This chip integrates a 10-bit ADC and an internal temperature sensor. However, the sensitivity in passive mode (without battery) is lower (−6.9 dBm) than the BAP mode (−15 dBm) that allows a longer rad range and data logging [7]. Semi-passive tags are microwave frequencies, or zero power tags are recently under intense research for sensing [10, 11].

At LF and HF, the radio link is established by near-field communication (NFC) because the distance is smaller than the wavelength. Therefore, the tag is in the near-field region, and the magnetic field decays proportionally to the square of the distance. Therefore, the communication between the loop antennas of the reader and the tag is produced by inductive coupling. However, at UHF and microwave bands, the communication is based on the modulation of the far fields, and hence the electromagnetic fields decrease and become inversely proportional to the distance. As a result, the read range of these tags is higher than those based on near-field communication [2, 4, 5].

Another recent approach to radio identification is the one known as chipless RFID [12, 13]. In these tags, the identification is done without a chip by a permanent modification of the structure that determines a specific electromagnetic signature in the frequency domain [12–15] or in the time domain [16, 17]. Initially, the main research efforts have been oriented to increase the number of bits that the electromagnetic structure can encode [13]. In frequency-coded chipless RFID, the number of bits is limited by the number of resonators with high-quality factors that can be integrated and detected in the bandwidth [13]. In time-coded chipless RFID, the number of bits is encoded in the length of the line, and it is limited by the time domain resolution of the radar that depends on its bandwidth and the losses of the lines [5]. The most important drawback of this technology is the detection of the tags. The change in the radar cross section (RCS) introduced by the chipless tag in frequency domain or in time domain is small compared with the clutter and objects in which the tag is attached. Therefore, in order to detect the tag, the background subtraction technique is often used in the literature. This technique consists of the subtraction of the background from the measurements using a previous saved measurement without the presence of the tag. In addition, the small perturbations introduced for the tag requires highly sensitive receivers; therefore, expensive vector network analyzers (VNAs) are often used as readers [18]. Another important drawback is the detection of several chipless tags in a small area due to the inexistence of an anti-collision protocol. The tags can only be identified by time gating if their spacing is higher than the spatial radar resolution [19] that is the function of the reader bandwidth. In order to mitigate these important issues, depolarizing tags [20] that reduce the clutter contribution and improve detection techniques have been developed in the literature [5, 21, 22]. In spite of these advances, the read range in frequency-coded chipless RFID is about 0.5–1 and 2–3 m for time-coded chipless tags. The inexistence of standardized readers in the market [18] and the limitations in the number of identification codes [13], in the read range, and in the cost (because it often uses high-frequency substrates, much more expensive than the substrates used in the inlay tags) are nowadays the challenges of this approach compared to UHF or other well-established RFID technologies. However, the interest of sensors based on chipless technology [23–26] is recently growing in those cases in which the robustness to harsh environments [26, 27] and the cost may be competitive with other sensor technologies. In sensor applications, the anti-collision issues are not critical in those applications in which the number of sensors is small, and few bits can be used for identification or other techniques can be employed. Small number of resonators can be used for identification, and other resonators can

be dedicated for sensing. The small number of resonators in chipless sensors simplifies its detection too and the bandwidth requirements [28].

Near-field communication technology at 13.56 MHz [29] is massively used for payment systems using NFC cards. Consequently, most smartphones include an NFC reader as it is shown in the exponential growing of number of NFC-enabled mobile devices depicted in **Figure 1** [30]. NFC employs electromagnetic induction between two loop antennas; therefore the range of these tags is constrained by the rapid drop of the magnetic field with the distance. However, enough energy can be harvested to feed low-power microcontrollers and sensors. As a consequence, the interest in the market of NFC-based sensors [31] is growing. Recently several manufacturers of NFC integrated circuits include the possibility of using energy harvesting (EH) in these integrated circuits. These components provide up to 3 mA at 2–3 V to feed low-power sensors [32]. These battery-less sensors can be interesting in numerous applications for short-range wireless reading of low-cost sensors. The use of mobiles as a reader for standardized tags enables a fast introduction of these sensors in the market. On the other hand, batteries contain toxic components that can contaminate foods and release waste pollutants to the environment [33]. Therefore, the use of battery-less sensors is a preferable choice in applications in which the devices are in contact with food or implanted in the body. In addition, in this last case, the replacement of the batteries is an important drawback.

Nowadays, besides the traditional applications of identification, the interest of RFID technology in applications such as sensing [34] and localization [35, 36] (e.g., for robot guidance) is growing. **Table 1** summarizes the main properties of passive RFID used for sensing (chipless RFID, NFC, UHF, and RFID) and a BLE as a representative wireless technology used in modern wearable applications. The key features of RFID technologies over active wireless technologies (such as Bluetooth or Zigbee) are the cost and the short setup time due to simpler communication protocol. The absence of battery, or its long lifetime in the case of BAP tags, is another valuable feature of the RFID technology. Depending on the read range required, NFC or UHF can be used. Nowadays, chipless RFID is a promising technology for short-range sensing. However, it is not mature enough for commercial use yet. Advanced sensors require additional processing; therefore, active wireless communication technologies with integrated microcontroller are needed. For wearable applications, BLE is a good option because this technology is available in smartphones. The cost of the reader is another important point that determines the selection of the technology. While the NFC and Bluetooth are low cost because most of the smartphones are equipped with NFC and Bluetooth modules, UHF readers are expensive, and therefore this technology is used in professional or logistic users but not for personal applications. In sensing applications where the read range of

Figure 1.
Number of NFC-enabled mobile devices worldwide from 2012 to 2018 (in million units) [30].

Feature	Chipless RFID	NFC	UHF RFID	BLE
Communication method	Backscattering far field	Backscattering near field	Backscattering far field	Transceiver far field
Read range	Typically, <50 cm for frequency-coded 2–3 m for time-coded UWB	1–2 cm for proximity cards with energy harvesting, 0.5 m for vicinity cards	Up to 15 m with inlay tags with −22 dBm read IC sensitivity Up to 3 m UHF sensors (with −9 dBm read IC sensitivity) Up to 30 m BAP	About 10 m
Energy source	Passive	Passive or semi-passive	Passive or semi-passive	Active
Tag price	Moderate	Low	Low	High
Reader cost	High, no commercial	Low, smartphone	High 1–2 k$	Low, smartphone
Standard	No	Yes	Yes	Yes
Universal frequency regulation	No, often used UWB	Yes, ISM	No, by regions	Yes, ISM
Tag size	Large	Medium	Medium	Small
Memory capacity	<40 bits	<64 kbits	96bits EPC, typically 512 bits for users (<64kbytes)	Several Kbytes depending on the microcontroller
ID rewritable	No	Yes	Yes	Yes
Setup time	—	Less than 0.1 s	Less than 0.1 s	Approx. 6 s
Energy harvesting	No	Approx. 10 mW	Few μW	No
Tag substrate	Low-loss microwave substrates	Low cost or FR4	Low cost or FR4	FR4
Tag flexibility	Depends on the substrate	Depends on the substrate	Depends on the substrate	No
Tag robustness	High	Low (inlays)	Low (inlays)	Moderate

Table 1.
Comparison of RFID technologies [32].

the Bluetooth is limiting, other wireless communication technologies such as Wi-Fi, Zigbee networks for medium range, or GPRS, Sigfox, LoRa, or NB-IoT for long range can be considered [37].

2. NFC energy harvesting

2.1 NFC communication

NFC employs electromagnetic induction between two loop antennas. It operates within the globally available unlicensed radio frequency ISM band of 13.56 MHz on ISO/IEC 18000-3 air interface at rates ranging from 106 to 424 kbit/s [2]. The communication between reader and tag is briefly described in **Figure** 2. Firstly, the reader transmits an unmodulated carrier to activate the tag (**Figure 2a**). The

receiver antenna at the tag is connected to the internal rectifier, which takes energy from the RF field to power up the tag electronics. After that, the reader sends commands by ASK modulating the carrier (**Figure 2b**), and the internal logic at the transponder demodulates the message. The tag transponder (which is assumed to be passive) responds using the passive load modulation technique (**Figure 2c**), by changing its antenna impedance [2, 29]. The passive load modulation spectrum consists of the RF carrier, two subcarriers at 12.712 and 14.408 MHz, and modulated sidebands on these two subcarrier signals (**Figure 3**). All the transmitted data are carried in the two sidebands.

An NFC tag IC is composed by two main blocks connected to the antenna ports (see **Figure 4**): the wireless power transfer unit that is responsible of harvesting the energy and powering the IC and the communication unit block that demodulates the messages and generates the clock for the transmission of data back to the reader. An RF limiter to protect the IC from a high-input voltage that could damage it, a rectifier, and a shunt regulator compose the WPT unit. The load modulator can be modeled as a shunt capacitance with the antenna. The IC impedance depends on the received power mainly due to the nonlinear behavior of the rectifier and the RF
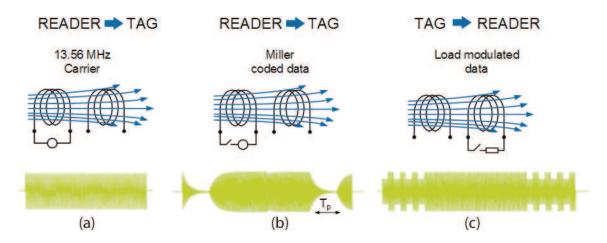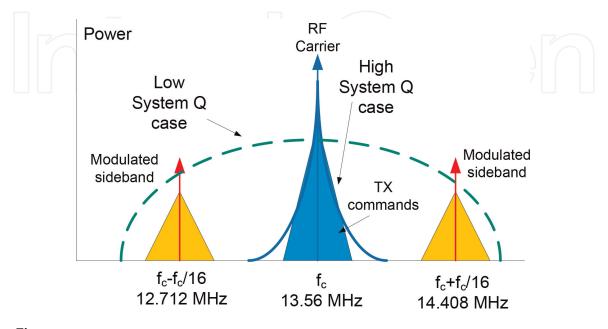

Figure 2.
Scheme of the communication between reader and tag: (a) power up the tag by the reader, (b) modulation of the carrier by the reader for transmission of the commands from the reader to the tag, (c) transmission the data from the tag to the reader by load modulation.

Figure 3.
A typical spectrum of an NFC system illustrating the reader command around the carrier frequency and the load modulation at the sidebands.
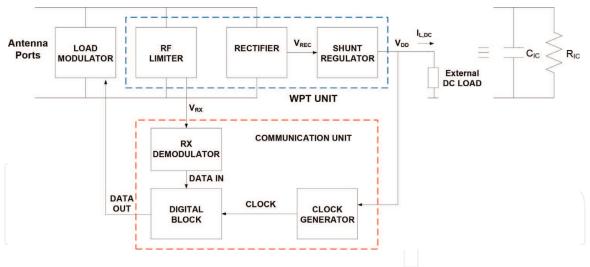
Figure 4.
Block diagram of NFC IC.

limiter. Therefore, a simplified model for the tag IC consisting of a nonlinear resistance R_{IC} in parallel with a capacitance C_{IC} that includes the parasitic elements is considered.

2.2 Commercial tags IC with energy harvesting

Nowadays, the most important manufactures offer NFC IC with energy-harvesting capabilities. These ICs have access to the internal output of the rectifier to feed external circuits such as microcontrollers or sensors. Some commercial NFC ICs with energy-harvesting mode are listed in **Table 2**. Most of them are compatible with standards ISO14443-3 or ISO15693 and can be connected to external microcontrollers using the I2C bus or serial-to-parallel interface (SPI). The internal EEPROM memory size to store the NFC Data Exchange Format (NDEF) message varies between 4 and 64 kbit. Although most NFC ICs are designed to be connected to a microcontroller, some models such as the MLX90129 from Melexis, the SL13 from AMS, and the SIC43x from Silicon Craft integrate an A/D for autonomous sensor acquisition without an external microcontroller, reducing the part count. In addition, the model RF430FRL152H from TI integrates a low-power microcontroller (MSP430) and a 14-bit A/D. The maximum sink current that can be drawn to power external devices connected to the EH output such as sensors or microcontrollers varies with the IC model and operation mode. Most of the models can configure different current levels depending on the range of magnetic field. The current to be provided depends on field strength, antenna size, and Q factor, but it is typically limited to the order of 5 mA with output voltages between 2 and 3 V for magnetic fields of the order of 3.5–5 A/m [32].
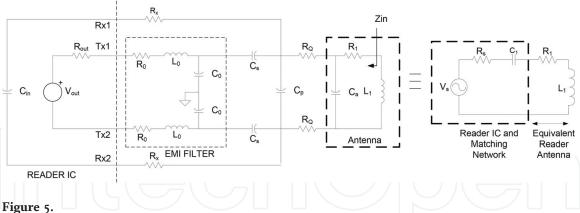
2.3 WPT in NFC systems and practical considerations

2.3.1 NFC reader

A simplified model of the RF front-end of an NFC reader transceiver is shown in **Figure 5**. The topology of the transmitter usually presents differential output, and it is connected to the loop antenna through a matching network to obtain the maximum transmitted power. The output resistance (R_{out}) is a function of the transmitter power, and the DC voltage determines the current consumption of the transmitter. The matching network is composed of a differential L matching network (C_s and C_p). The current that flows through the loop antenna produces the

IC model (manufacturer)	Energy harvesting Max. sink current and typical voltage	Standard	ADC	Interface bus	Memory and other comments
M24LR-E-R ST25DV-I2C (STMicro-electronics)	*6 mA/3 V*	*ISO15693*	*No*	*I2C*	*4–64kBit*
NT3H1101 NT3H1201 (NXP)	*5 mA/2 V*	*ISO14443-3*	*No*	*I2C*	*8kBit/16kBit*
NF4 (EM Microelectronics)	5 mA/3.6 V	ISO14443A	No	SPI	8kBit/32kBit/64KBit
GT23SC6699–1/2 (Giantec Semiconductor)	NA/3.2 V	ISO14443-3	No	I2C	8kBit/16kBit
SIC4310 SIC4340 SIC4341 (Silicon Craft)	10 mA/3.3 V	ISO14443A	No Yes	UART	220 bytes EEPROM
AS3953A (AMS AG)	5 mA/2 V	ISO14443A-4	No	SPI	1KBit
SL13 (AMS AG)	4 mA/3.4 V	ISO15693	Yes	SPI	8 kBit temperature sensor integrated
MLX90129 (Melexis)	5 mA/3 V	ISO15693	Yes	SPI	4kBit
RF430FRL152H (Texas Inst.)	NA/3 V	ISO15693	Yes	I2C/SPI	MSP430 2kB FRAM

Table 2.
Main features of some commercial NFC ICs with energy harvesting [32].

Figure 5.
Model of the reader including the matching network, EMI filter, and antenna model and the simplified equivalent circuit model (right).
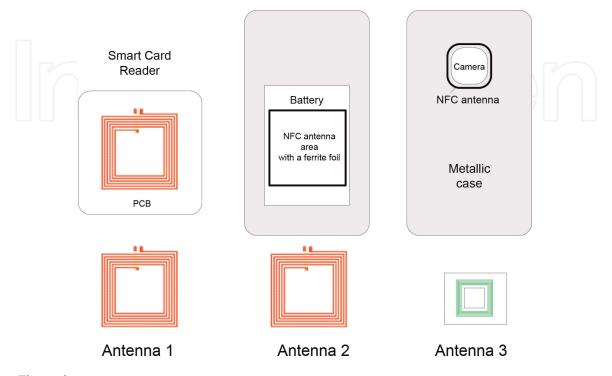
magnetic field. In order to fulfill the emission regulations, a low-pass LC filter to reduce the spurious emission at the second harmonic is included. The receiver shares the loop antenna with the transmitter; therefore, two series resistances R_x are often added to attenuate the signal, avoiding the AC voltage at the receiver input to exceed a limit value and saturating it. Sometimes, a capacitive splitter is used for that purpose. The input impedance of the receiver is mainly capacitive, and it is modeled with the capacitance C_{in} in **Figure 5**. Although the overall impedance of the R_x and C_{in} is high, the effect of the receiver impedance must be considered in the design of the matching network. The steps to design this matching network can be found in [32]. In addition, recently, modern transceivers such as the ST25R391x incorporate an automatic antenna tuning method, enabling the matching network design in which C_p may be modified by switching an external bank of capacitors [38].

Printed loop antennas are used in NFC reader designs. There is a great variety of them depending on the reader type, but they are often designed to maximize the coupling with a payment card. Therefore, relatively large antennas between 4 and 5 cm square loops are integrated. The quality factor of these printed antennas is often high (more than 70). As the quality factor of the transmitter determines its bandwidth B ($B = f_c/Q$), the quality factor (Q_T) must be reduced to allow the transmission of the sidebands of the carrier. To this end, two series resistances R_Q are added at the input. The maximum quality factor of the transmitter is limited by the duration of the pause T_p in the modified Miller bit coding (see **Figure 2**):

$$Q_{Tmax} = f_c \cdot T_p \tag{1}$$

The quality factor is limited to 40 and 128, for standards ISO 14443 and ISO 15693, respectively (35 and 100 considering design tolerances). Condition (1) represents an additional restriction for energy harvesting compared with other WPT systems for battery charging (with or without very small communication rate) where high Q coils can be used in the transmitter and receiver to increase the power efficiency.

Despite the transmitter's complexity, it can be modeled using a simplified Thevenin equivalent circuit tuned at f_c = 13.56 MHz, used for circuit analysis (see **Figure 5**, right). The parasitic capacitance of the transmit antenna is included within the equivalent circuit. The relatively low-quality factor of the coils simplifies the antenna reader design. Antenna inductance varies typically between 1 and 3.5 µH. Several formulas for inductance calculation can be found depending on the shape of the printed antenna [39, 40]. In addition, the inductance and the equivalent resistance (or quality factor) can be analyzed using electromagnetic simulators such as Keysight ADS, HFSS, or CST studio, among others. The main challenge in the antenna design arises when it must be integrated into the reader case, since the proximity of metallic parts or other components (e.g., displays, batteries, or PCB boards) can modify the inductance and the parasitic capacitance. The worst case is the presence of NFC transceiver in modern smartphones, due to space limitations. **Figure 6** considers three different types of reader antennas including the typical

Figure 6.
Typical NFC reader antennas [41]: Antenna over a PCB (antenna 1), antenna on top of a mobile battery (antenna 2), and antenna around the camera hole (antenna 3).

Parameter	Antenna 1	Antenna 2	Antenna 3
Loop area (mm × mm)	50 × 50	50 × 50	25 × 25
Trace width (mm)	0.7	0.7	0.25
Spacing between traces (mm)	0.7	0.7	0.25
Number of turns	6	6	8
Substrate relative permittivity	4.7	4.7	3
Substrate thickness (mm)	0.8	0.8	0.1
Ferrite relative permeability[*]	—	150-j5	150-j5
Inductance (μH)	2.68	3.92	3.63
Self-resonance frequency (MHz)	77.0	37.4	79.05
Quality factor at 13.56 MHz	153	132	74
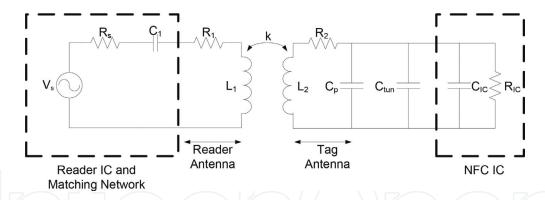
Antenna 1 and Antenna 2 have the same dimensions, but Antenna 2 has a sheet of ferrite.
[*]100 μm thickness with 50 μm of adhesive plastic sheet of MHLL12060-200 from Laird (with μ_r = 150-j5) is considered.

Table 3.
*Dimensions and simulated parameters of the reader antennas of **Figure 6**.*

locations of the NFC antenna into the smartphone [41]. **Table 3** compares the main parameters analyzed. Antenna 1 corresponds to a simple printed antenna over a PCB such as used on readers connected to PC through the USB port. Antenna 2 corresponds to a typical smartphone with a plastic case in which the antenna is attached to the battery pack of the mobile. A sheet of ferrite isolates the traces from the metal on the bottom plane. Antenna 3 is known as Murata solution [42], and it is based on the integration of the loop antenna around the hole of the camera. The magnetic field generated or collected by a coil over or close to a metallic surface is almost parallel to this surface. Hence the magnetic flux is concentrated in the proximity of the coil [43], whereas it is zero in its center because of the cancelation of the field produced by the image currents with opposite sign. The effect is a considerable reduction in the read range and the increasing of the losses. A layer of ferrite material is placed under the coil, in order to isolate the antenna in the presence of metal. Modern sintered ferrite sheets with Re(μ_r) between 100 and 190 and Im(μ_r) losses typically of 5–10 at 13.56 MHz can be found in the market (e.g., MHLL12060-000 from Laird). As it can be appreciated in **Table 3**, the high magnetic permeability (μ_r) increases the inductance depending on the thickness of the ferrite foil. The effect of the ferrite loss produces an increasing of the antenna resistance and therefore a reduction of the antenna quality factor as it can be seen in **Table 3**. This is not an inconvenience so that it will only be necessary to readjust the matching network. Consequently, the inclusion of a ferrite layer modifies the field boundary conditions, making the magnetic field almost perpendicular, creating a scenario similar to the case of free space [32, 44].

2.3.2 Tag design considerations

Figure 7 shows a simplified equivalent circuit of the NFC system. The transmitter and the IC are modeled with the Thevenin model of **Figure 5** and its equivalent input impedance (**Figure 4**), respectively. The tag antenna is modeled with an inductance L_2, its equivalent resistance R_2 that takes into account the antenna losses, and its parasitic capacitance C_p. The coupling between the transmitter and receiver coils allows the transfer of energy between the transmitter and the tag.

Figure 7.
Wireless power transfer model between the reader and the tag.

In order to achieve high efficiency, the resonance frequency of the tag must be adjusted to the operation frequency (13.56 MHz).

The design of an NFC tag is relatively easy. The resonance frequency is obtained from the simplified equivalent circuit of **Figure 4**, and it is given by:

$$f_r \approx \frac{1}{2\pi \sqrt{L_2 \left(C_{IC} + C_p + C_{tun} \right)}} \qquad (2)$$

where L_2 is the inductance of the tag antenna, C_{IC} is the equivalent capacitance of the NFC IC, C_p is the parasitic capacitance of the antenna and interconnections, and C_{tun} is an additional tuning capacitance connected in parallel at the input, used to adjust the resonance frequency. C_{IC} is nonlinear and varies about 5% with the received power. The typical values of C_{IC} provided by the IC manufactures vary between 20 and 50 pF when low-input levels are applied on them.

Similar to the transmitter, the loaded quality factor of the tag (Q_{2L}) must be low enough to achieve the communication bandwidth, avoiding the attenuation of the modulation of the subcarrier in the backscattering link. Therefore, the maximum value of Q_{2L} is approximately $Q_{2L} = 8\pi \approx 25$ [29]. The loaded quality factor (Q_{2L}) is the hyperbolic average of the quality factor of the tag's antenna (Q_2) and the loaded quality factor of the IC (Q_L). Therefore, for typical values of printed loop antennas ($Q_2 > 50$), the loaded quality factor is approximately Q$_L$:

$$Q_{2L} = \frac{1}{\frac{1}{Q_2} + \frac{1}{Q_L}} \approx Q_L \qquad (3)$$

$$Q_L = \frac{R_{IC}}{\omega L_2} \qquad (4)$$

Consequently, the tag quality factor $Q_{2L} <$ Q$_{2L\text{max}}$ if the following condition is fulfilled:
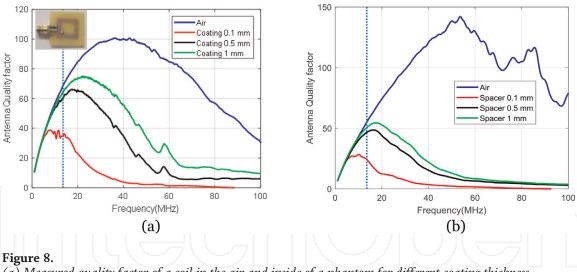
$$L_2 > \frac{R_{IC}}{\omega_0 Q_{2L,\,max}} \qquad (5)$$

R_{IC} is highly nonlinear and decreases with the input level. R_{IC} takes typical values between 1500 and 400 in commercial ICs for the activation input level [45]. Therefore, condition (5) can be easily fulfilled for tag inductances higher than 0.7 μH, and in consequence, tag design is simple because it only is necessary to tune the resonance frequency with the capacitance C_{tun} for the desired loop antenna.
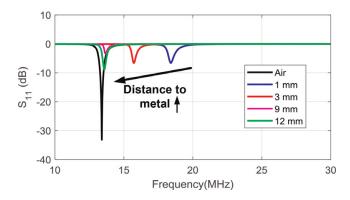
To this end, it is important to know the environment in which the tag will be used. The presence of high-permittivity materials such as the body or, for example,

on wearable or implanted applications can detune the tag. These materials are nonmagnetic; therefore, they do not modify the loop inductance, but change the parasitic capacitance, reducing the resonance frequency and increasing losses. **Figure 8a** shows the measured results of an implanted antenna in a phantom that consists of a piece of pork steak. The antenna is a 15 × 15 mm square coil consisting of six loops, printed in duplicates on each of the layers of a FR4 board whose thickness is 0.8 mm. The introduction of a low-permittivity cover (e.g., silicone, ε_r = 3) allows to reduce the losses of the phantom when the thickness is larger than 1 mm. Similar results are found for a coil close to the body surface (**Figure 8b**) considering a low-permittivity spacer (ε_r = 3) located between the coil and the body. Here the coil is a 25 × 25 mm square consisting of four loops printed on a thin flexible substrate (Ultralam 3000, thickness 100 μm).

Another typical situation is the detuning due to the presence of nearby metal surfaces. If the NFC sensor is going to work on a metallic surface, the antenna can be isolated using a ferrite foil as in the case of the reader. But the typical situation takes place in the tags that will be read by smartphones with a metallic case. In this case, the inductance of the tag will be reduced by the presence of the metal due to the opposite image currents induced on it. The result is a detuning of the tag as can be shown in **Figure 9**. In order to check if a tag is correctly tuned, a test coil can be connected to the port 1 of a vector network analyzer. An absorption peak will be observed at the resonance frequency if the test coil is located close to the tag (but sufficiently spaced to avoid strong coupling between the coils). **Figure 10** shows the inductance of a coil as a function of the metal distance. A considerable reduction of
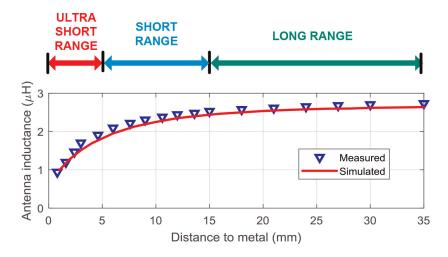

Figure 8.
(a) Measured quality factor of a coil in the air and inside of a phantom for different coating thickness, (b) measured quality factor of a thin coil over the skin as a function of the spacer thickness.

Figure 9.
Measured S_{11} of the test antenna as a function of frequency for different distances between the tag and the mobile [32].

its value is observed. Therefore, the tag must be tuned depending on the application and the desired read range of the tag.

The area available for the antenna depends on the application. For example, **Table 4** shows the design of a tag sensor using the coil of **Figure 10** and an M24LR04E-R IC from ST for short range (5 mm) and long range (15 mm). For long ranges (distances higher than 15 mm), the inductance and the other antenna parameters (resistance and capacitance) are nearly constant and close to the values of the free space case. The tuning capacitor (C_{tun}) that must be mounted in parallel at the input of the NFC IC is obtained from (2), and it is approximately 25 pF. However, for short read range applications in the presence of metal, the values of inductance for a distance of 5 mm must be considered. In this case, the tuning capacitance must be increased up to 36 pF. The inductance for each case is obtained from the measured impedance with the VNA, and the parasitic capacitance (C_p) is obtained from the self-resonance frequency of the antenna (without considering the tuning capacitor). If the antenna cannot be measured, e.g., due to the lack of laboratory instruments, the tuning capacitance can be obtained considering that the

Figure 10.
Simulated and measured antenna inductance as a function of the distance to a ground plane for a 50 × 50 mm loop antenna with 0.7 mm trace width and six turns, manufactured on a 0.8-mm-thick FR4 [32].

Parameter	Tuning for short range (5 mm)	Tuning for long range (15 mm)
Loop area (mm × mm)	50 × 50	50 × 50
Trace width (mm)	0.7	0.7
Spacing between traces (mm)	0.7	0.7
Number of turns	6	6
FR4 substrate thickness (mm)	0.8	0.8
Metal thickness (μm)	34	34
Chip capacitance C_{IC} (pF)	27.5	27.5
Inductance L_2 (μH)	2.68	3.92
Self-resonance frequency (MHz)	52.9	55.7
Antenna quality factor Q_2	87	118
Parasitic capacitance C_p (pF)	2.3	1.7
Tuning capacitance C_{tun} (pF)	36	25

Table 4.
Example of design for short-range application (5 mm) and long-range application (15 mm).

nominal inductance (value measured or computed in free space) decreases about 16% for short-range case. For very short ranges, the coupling coefficient k between the transmitter and tag antennas is very high (typically $k > 0.1$). Therefore, the input impedance at the transceiver increases (see **Figure 7**) due to the loading effect of the tag, and it is detuned because the matching network is designed considering that it is far from the reader and hence uncoupled to it. This is the reason why sometimes the tags are read worse when are on contact or very close to the reader than when are more spaced.

2.3.3 WPT and read range

The communication in an NFC system can be limited by the uplink (reader to tag) when the tag does not receive enough energy to power the transponder IC or by the downlink (tag to reader) if the backscattered level received at the NFC reader is not sufficiently high to demodulate the message. For an NFC IC equipped with energy harvesting, the main limitation is the WPT in the uplink because it is necessary to provide higher energy than in a conventional NFC IC without energy harvesting. Thus, the read range in NFC tags with the EH mode activated is lower than the range for reading a previously stored data in the memory.

At this point it is interesting to take into account the factors that limit the read range of an EH NFC sensor. To this end, the wireless power transfer between the reader and tag can be analyzed considering the circuit of **Figure 7**. Analytical formulas found in the literature or a circuit simulator such as Keysight ADS can be used. In this model, $L1$ is the reader antenna inductance and R_1 is its losses. C_1 is the equivalent series capacitance that allows the circuit to resonate at 13.56 MHz. $L1$ and $R1$ can be obtained from the measurement of the antenna impedance or from electromagnetic simulations. R_s is the Thevenin output resistance, and it is chosen to achieve the maximum loaded Q factor in the transmitter to ensure the communication. As the reader in the smartphone is designed to read both ISO 14443A and ISO 15693 standards, the Q_T is often limited to 35. Therefore, R_s is obtained from the loaded quality factor of the transmitter at 13.56 MHz ($R_s = \omega L_1/Q_T-R_1$). The inductance L_2 in series with a loss resistance R_2 is used to model the tag antenna.

A key parameter is the mutual inductance M between the coils, as a function of the distance. The coupling coefficient k is obtained from the Z parameters from electromagnetic simulations or S parameters measurements performed with VNA:

$$k = \frac{M}{\sqrt{L_1 L_2}} = \frac{|Im\,(Z_{12})|}{\sqrt{Im\,(Z_{11}) \cdot Im\,(Z_{22})}} \tag{6}$$

Figure 11 compares the simulated coupling coefficient for each reader antenna as a function of the distance between the tag and reader antenna. Antenna 1 has been used as the tag antenna since it has a size similar to a smart card. The simulations have been done using Keysight Momentum. The coupling coefficient is obtained using (6) from the simulated Z parameters. **Figure 11** shows a similar coupling coefficient for Antennas 1 and 2 (see **Figure 6**). Therefore, the introduction of the ferrite foil effectively mitigates the effect of the metal. On the other hand, the coupling coefficient of Antenna 3 (**Figure 6**) is smaller than in the previous cases because its area is the smallest.

The circuit of **Figure 7** can be analyzed both analytically [46] or using a circuit simulator (e.g., Keysight ADS). In any case, the NFC IC is considered linear and modeled with its equivalent circuit. The values of R_{IC} and C_{IC} depend on the power.

In addition, the manufacturer does not often give R_{IC}. This equivalent circuit can be measured using a VNA. However, the output level of commercial VNA does not achieve the typical level in a tag under real conditions. A modified high-power VNA with an external reflectometer and a power amplifier can be used, as it is proposed in Refs. [45, 47]. An alternative setup with an oscilloscope has been recently presented in [48]. However, these setups are not often available for the users interested in the design of NFC-based sensors. In order to estimate the maximum read range, the value of R_{IC} at that distance must be known. It can be estimated from the minimum average magnetic field, H_{min}. This is the threshold average
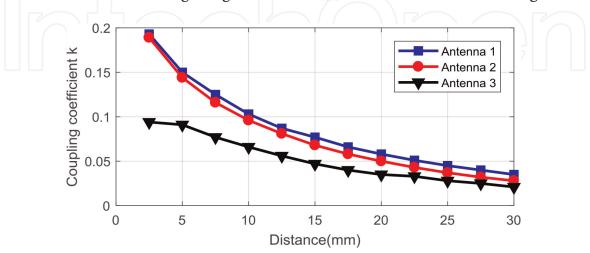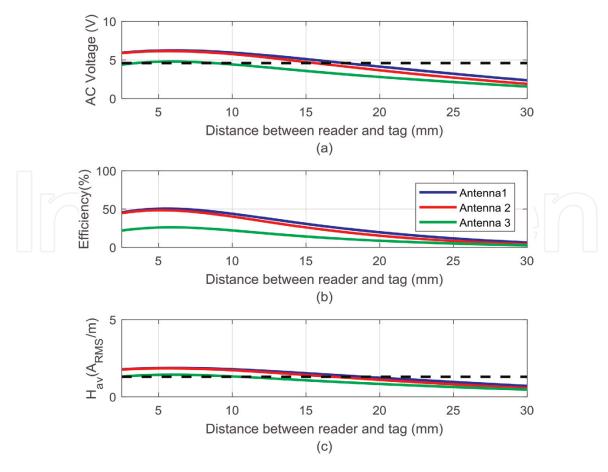

Figure 11.
Simulated coupling coefficient between a tag using antenna 1 and different reader antennas of **Figure 6**.

Figure 12.
(a) Simulated voltage at the input of the tag at 13.56 MHz (V_{AC}), (b) efficiency, and (c) average magnetic field H_{av}, as a function of the distance for 20 dBm of transmitted power. The threshold limit is shown in dashed line.
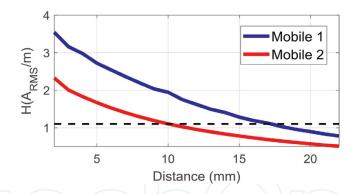
Figure 13.
Measured average magnetic field H$_{av}$(A_{RMS}/m) for a tag using antenna 1 as a function of the tag-to-reader distance for two mobile models.

magnetic field that ensures the RF to DC conversion at the read range and can be computed from Ref. [45]:
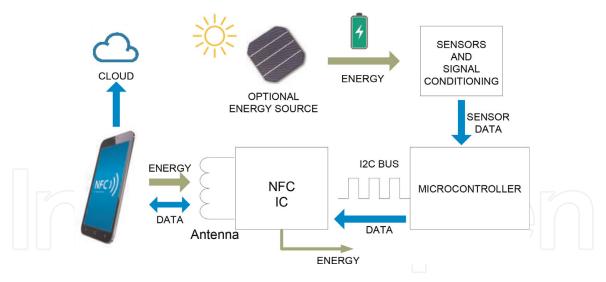
$$H_{min} \approx \frac{\sqrt{\left[1-\left(\frac{f}{f_r}\right)^2\right]^2 + \frac{1}{Q_{2L}^2}}}{2\pi f \mu_0 A \cdot N} \cdot U_{min} \tag{7}$$

where f_r is the resonance frequency of the tag, A is the loop area, N is the number of loops, and U_{min} is the minimum AC threshold voltage at the IC input required for the NFC IC operation. Therefore, H_{min} depends only on the tag parameters, and it can be considered a figure of merit of the tag. It can be experimentally found measuring the average magnetic field generated by the reader as a function of the distance between the tag and reader. A measurement procedure can be found in [32, 41]. U_{min} can be measured with an oscilloscope using a probe with low capacitance at the maximum distance where EH is activated.

Taking into account the coupling coefficients of **Figure 11**, **Figure 12** compares simulated results for the antennas considered in **Figure 6**. It is assumed that the transmitter power is 20 dBm and that EH output is activated if the AC voltage at the input of the rectifier is high enough. In these conditions, the average field is equal to H_{min}. Considering U_{min} = 4.8 V, H_{min} = 1.2 A$_{RMS}$/m, and R$_{IC}$ = 550 Ω, a distance between 12 and 18 mm is obtained. This estimation is in agreement with measurements of received H_{av} for a tag using the same antenna than in the simulation. Experimentally, a value of $H_{min} \approx$ 1.1 A$_{RMS}$/m (see **Figure 13**) corresponding to an EH range of 10 and 17 mm has been obtained, depending on the mobile used.

3. NFC sensors

Figure 14 shows the block diagram of an NFC-based data logger assisted with a complementary (optional) energy source (e.g., a solar cell). It is composed of an antenna that receives the interrogation signal emitted from a reader, usually, a mobile equipped with an NFC reader, an NFC integrated circuit, a microcontroller, and the sensor and its conditioning electronics. **Table 2** shows that there are several commercial NFC ICs with energy-harvesting capabilities available in the market. These devices can operate in two modes: battery-assisted (semi-passive) and battery-less (passive). Battery-assisted devices are used in data logger applications where stand-alone continuous and autonomous monitoring is necessary. The NFC sensor is fed from a battery or assisted from an additional harvesting source. These devices can communicate with external microcontrollers using I2C or SPI interface.

Figure 14.
Block diagram of a green NFC-based sensor system.

In the passive operation mode, the integrated NFC circuit is in charge of capturing the energy from the RF signal, rectifying it and extracting energy for the electronic circuits, microcontroller, or sensors. Sensors based on NFC IC with energy harvesting may operate in both modes: in semi-passive mode until the battery is exhausted and thereafter in passive mode. Data are stored in the EEPROM of the NFC IC to be read when the user taps the sensor. It should be highlighted that for tags in battery-less mode, data can only be updated with a new sensor reading in the presence of field from the reader. Another challenge is the amount of power that can be harvested from the RF signal. According to market research summarized in **Table 2**, commercial ICs can provide up to 15 mW. Despite this figure, battery-less sensors based on NFC have a wide range of applications. The most important key is that a specific reader is not required because the own smartphone equipped with NFC can be used as reader, and the data can be uploaded to cloud services using the Internet connectivity of the mobile. This fact is probably the important factor for the diffusion of this technology as can be derived from the large number of battery-less sensors based on NFC that are recently reported in the literature. Next section will review some examples.

3.1 Survey of NFC-based sensors

Several temperature sensors based on NFC have been proposed in the literature for different applications. In the pioneering works, based on NFC-WISP [49, 50] due to the inexistence of commercial NFC IC with energy harvesting, the rectification was performed with an external full-wave rectifier with discrete diodes. NFC-WISP communicated using the ISO-14443 protocol implemented in a low-power microcontroller (TI MSP430). As an option, the data could be shown in an E-ink display.

The monitoring of environment temperature in a cold chain or body temperature without using batteries that contain toxic products has aroused great interest. Several temperature sensors based on commercial IC such as MLX90129 [51] or RF430FRL152H [52, 53] have been reported in the literature for these applications. Other physical magnitudes can be measured with NFC sensors. For example, [54] reports a wireless tire pressure sensor based on a custom ASIC compatible with ISO14443 protocol.

A soil moisture battery-less NFC sensor for low-cost irrigation control at home, in a greenhouse, or at a garden center has been presented in [55]. The tag is based on

an M24LR04E-R from ST connected to a low-cost microcontroller (ATtiny85 from Atmel). Volumetric water content of soil is obtained from capacitance measurement based on a low-power timer 555 working as an oscillator and a diode detector whose output is measured by the ADC of the microcontroller. Additionally, the temperature is measured using an I2C temperature sensor (LM75A), while air humidity is detected by reading the analog output from the HIH-5030 humidity sensor from Honeywell. The external circuitry requires less than 1 mA at 3 V to operate. **Figure 15** shows an image of the soil volumetric water content sensor inserted in a flower pot, the mobile app that shows the information in the screen and a comparison between the measured and the real volumetric water content (soil moisture) [55].

A second example is a smart diaper [56]. The tag is based on the M24LR04E-R from ST and an ATtiny85 from Atmel. The microcontroller senses the capacitance between two electrodes based on the discharge time of an RC circuit. The capacitance changes as a function of the urine level, as it is shown in **Figure 16**. Chemical sensors inserted in NFC-based tags have also been proposed. The presence of gas sensors based on functionalized CWNT that change the resonance frequency of an NFC has also been proposed in [57].

Another advantage of NFC technology over other types of RFID working at UHF frequencies is that the NFC antennas can be designed to be compatible with the body. The effect of the body on NFC antennas is lower than at UHF band, where a considerable reduction of antenna efficiency and therefore the read range is experienced. Therefore, although the body losses reduce the quality factor of the coil and can detune the resonance frequency, the introduction of a small spacer can mitigate these effects, as shown in the previous section. Several wearable NFC-based sensors can be found in the literature that exploits this fact. In addition, the short read range inherent in the NFC technology provides a degree of privacy and security over undesired access to sensible information by nearby third parties [58, 59]. Prototypes of patches to perform measurements of body temperature based on commercial NFC IC can be found in [52, 53]. Another example is a prototype for monitoring the degree of hydration based on Melexis MLX90129 [60]. This sensor measures the concentration of NaCl in sweat, reading the surface temperature and sensing the potential difference between two electrodes. A noninvasive, NFC pH sensing system for monitoring wound healing and identifying the possibility of early-stage
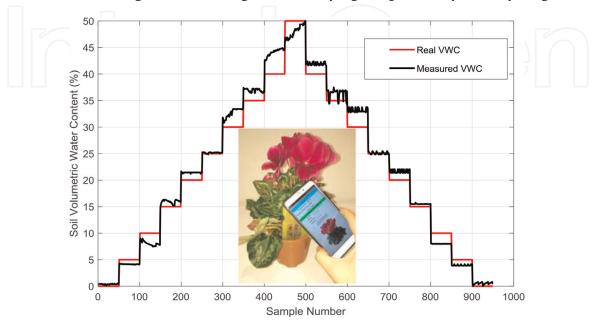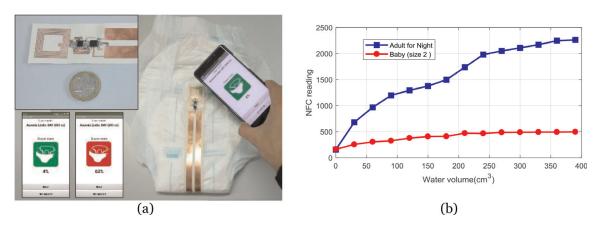

Figure 15.
Comparison of the volumetric water content (VWC) obtained with the sensor and real [55].
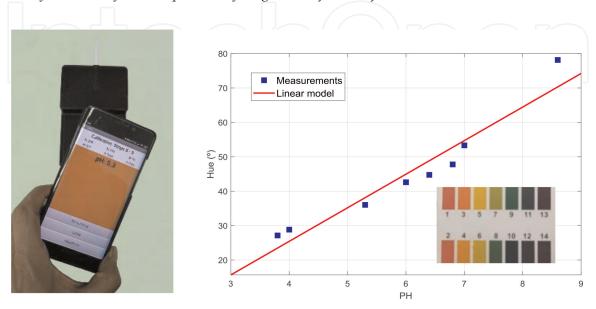
infection is reported in [61]. A low-power CMOS ISFET array for pH sensing is inductively powered using SIC4310 from Silicon Craft NFC IC in [62].

The authors have demonstrated that colorimetric measurements can be done with battery-less NFC. The advantage over other methods based on cameras is that the illumination conditions are similar, and therefore the measurements have higher repeatability and accuracy. A prototype of NFC colorimeter with a low-cost color light-to-digital TCS3472 converter from TAOS is integrated with an ST M24LR04E-R NFC IC and a microcontroller (see **Figure 17**). It is used to measure the change in color of pH tires [41]. The same method can be used for other sensors based on the measurement of the color changes due to another sensitive chemical component (e.g., urine tests). **Figure 17** shows an image of the prototype and a comparison of the measured hue component as a function of the pH, showing that a simple linear model can be employed for pH calibration. The same NFC colorimeter is adapted to the design of a color-based classification system for grading the ripeness of fruit in [63] (**Figure 18**).

Finally, another application of NFC sensors is implantable medical devices (IMDs). Long-term implantable continuous glucose monitoring based on custom ASIC has been reported in [64, 65]. Wireless communication with IMDs is fundamental for monitoring and the reconfiguration of these devices to reduce the
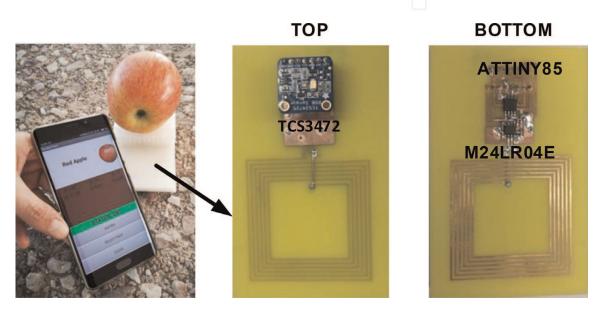

(a)   (b)

Figure 16.
(a) Photograph of the layout of the tag and the screen of the mobile app. (b) NFC reading as a function of the level of saline water for two diapers (adult for night and day and baby size 2).
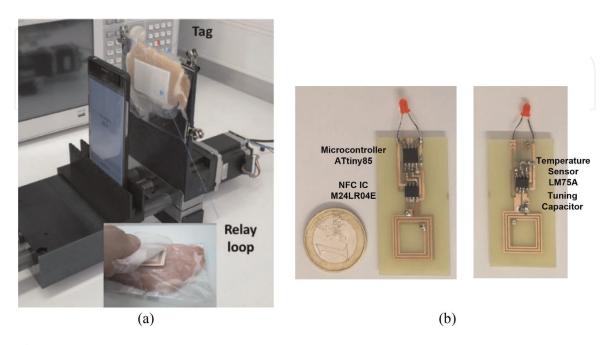

Figure 17.
Photograph of an NFC PH sensor from the measurement of the color of a strip with the android application and relation between the measured hue and the pH [41].

surgical operations [58]. Due to the size of the implanted coil, the coupling coefficient with the antennas integrated into the mobile is small, resulting in a short read range. One method to improve the readability with a modern smartphone and to increase the energy-harvesting range is including a relay coil on the body surface integrated on a patch. **Figure 19a** shows the setup for measuring the average magnetic field and a prototype of implanted NFC sensor integrating a LED, a temperature sensor, and a microcontroller as proof of concept (**Figure 19b**). **Figure 20** shows the measurements with a commercial mobile of the average magnetic field as a function of the distance of an implanted coil of 15×15 mm within a phantom of pork steak for different depths of the implanted tag. Two systems are compared: the conventional two-coil system and a three-coil system where a relay resonant coil is on a patch over the skin. Using the last system, implanted NFC

Figure 18.
Photograph of the NFC tag within the 3D printed enclosure in real application to detect apple ripeness and top/bottom photographs of the prototype.

(a)   (b)

Figure 19.
(a) Setup used for the measurement of the average magnetic field, (b) photograph of a designed tag for testing: Top view (left) and bottom view (right).
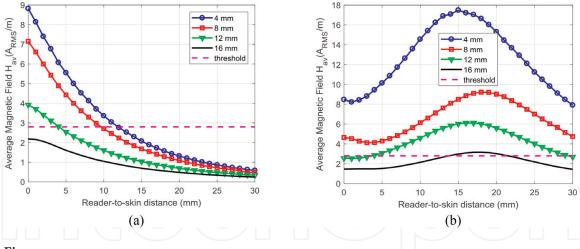
Figure 20.
Measured average magnetic field as a function of the mobile to skin distance for an implanted tag in a phantom at different depths between 4 and 16 mm for the two-coil system (a) and the three-coil system with a resonant relay loop on the skin (b). The threshold H_{min} is shown in dashed line.

sensors can be powered by conventional smartphones at a depth up to 16 mm and read at distance between 1 and 2 cm from the skin.

4. Conclusion

The availability in the market of low-cost near-field communication devices with energy-harvesting capabilities allows to feed small sensors enabling the development of low-cost battery-less sensors. One important advantage over other RFID is that additional readers are not required since most of the modern smartphones incorporate NFC readers. The limited read range for a selected number of applications is an advantage rather than a drawback because it ensures the privacy and improves the security under undesired access to sensible information by nearby third parties. In this chapter, an overview of recent advances in the field of battery-less NFC sensors at 13.56 MHz is provided, and it also briefly compares these sensors to other short-range RFID technologies. After reviewing power transfer in NFC, recommendations are made for the practical design of NFC-based sensor tags and NFC readers. A list of commercial NFC integrated circuits with energy-harvesting capabilities is also provided. A survey of recent battery-less NFC-based sensors for different applications has been done showing that conventional low-power sensors can be integrated within NFC tags for the new generation of IoT devices.

Acknowledgements

Author details

Antonio Lazaro*, Marti Boada, Ramon Villarino and David Girbau
Department of Electronic, Electric and Automatic Control Engineering,
Rovira i Virgili University, Tarragona, Spain

*Address all correspondence to: antonioramon.lazaro@urv.cat

IntechOpen

References

[1] Landt J. The history of RFID. IEEE Potentials. 2005;**24**(4):8-11. DOI: 10.1109/MP.2005.1549751

[2] Finkenzeller K. Rfid Handbook: Fundamentals and Applications in Contactless Smart Cards, Radio Frequency Identification and Near-Field Communication. 3rd ed. Chichester: Wiley-Backwell; 2010. ISBN: 978–0470695067

[3] Want R. An introduction to RFID technology. IEEE Pervasive Computing. 2006;**5**(1):25-33. DOI: 10.1109/MPRV.2006.2

[4] Rao KVS, Nikitin PV, Lam SF. Antenna design for UHF RFID tags: A review and a practical application. IEEE Transactions on Antennas and Propagation. 2005;**53**(12):3870-3876. DOI: 10.1109/TAP.2005.859919

[5] Nikitin PV, KVS R. Performance limitations of passive UHF RFID systems. In: 2006 IEEE Antennas and Propagation Society International Symposium. Albuquerque: IEEE; 2006. pp. 1011-1014. DOI: 10.1109/APS.2006.1710704

[6] Sample AP, Yeager DJ, Powledge PS, Mamishev AV, Smith JR. Design of an RFID-based battery-free programmable sensing platform. IEEE Transactions on Instrumentation and Measurement. 2008;**57**(11):2608-2615. DOI: 10.1109/TIM.2008.925019

[7] Nappi S, Mazzaracchio V, Fiore L, Arduini F, Marrocco G. Flexible pH sensor for wireless monitoring of the human skin from the Medimun distances. In: 2019 IEEE International Conference on Flexible and Printable Sensors and Systems (FLEPS). Glasgow: IEEE; 2019. pp. 1-3. DOI: 10.1109/FLEPS.2019.8792291

[8] Ramos A, Lazaro A, Girbau D. Semi-passive time-domain UWB RFID system. IEEE Transactions on Microwave Theory and Techniques. 2013;**61**(4):1700-1708. DOI: 10.1109/TMTT.2013.2247056

[9] Wang B, Law M-K, Yi J, Tsui C-Y, Bermak A. A −12.3 dBm UHF passive RFID sense tag for grid thermal monitoring. IEEE Transactions on Industrial Electronics. 2019;**66**(11): 8811-8820. DOI: 10.1109/TIE.2019.2891447

[10] Lorenzo J, Lazaro A, Villarino R, Girbau D. Modulated frequency selective surfaces for wearable RFID and sensor applications. IEEE Transactions on Antennas and Propagation. 2016;**64**(10):4447-4456. DOI: 10.1109/TAP.2016.2596798

[11] Memon ML, Saxena N, Roy A, Singh S, Shin DR. Ambient backscatter communications to energize IoT devices. IETE Technical Review. 2019: 1-15. DOI: 10.1080/02564602.2019.1592717

[12] Preradovic S, Balbin I, Karmakar NC, Swiegers GF. Multiresonator-based chipless RFID system for low-cost item tracking. IEEE Transactions on Microwave Theory and Techniques. 2009;**57**(5): 1411-1419. DOI: 10.1109/TMTT.2009.2017323

[13] Preradovic S, Karmakar NC. Design of fully printable planar chipless RFID transponder with 35-bit data capacity. In: 2009 European Microwave Conference (EuMC). Rome: IEEE; 2009. pp. 013-016. DOI: 10.23919/EUMC.2009.5296182

[14] Vena A, Perret E, Tedjini S. Chipless RFID tag using hybrid coding technique. IEEE Transactions on Microwave

Theory and Techniques. 2011;**59**(12): 3356-3364. DOI: 10.1109/TMTT.2011. 2171001

[15] Costa F, Genovesi S, Monorchio A. A chipless RFID based on multiresonant high-impedance surfaces. IEEE Transactions on Microwave Theory and Techniques. 2013;**61**(1):146-153. DOI: 10.1109/TMTT.2012.2227777

[16] Hu S, Law C, Dou W. A balloon-shaped monopole antenna for passive UWB-RFID tag applications. IEEE Antennas and Wireless Propagation Letters. 2008;**7**:366-368. DOI: 10.1109/ LAWP.2008.928462

[17] Lazaro A, Ramos A, Girbau D, Villarino R. Chipless UWB RFID tag detection using continuous wavelet transform. IEEE Antennas and Wireless Propagation Letters. 2011;**10**:520-523. DOI: 10.1109/LAWP.2011.2157299

[18] Garbati M, Perret E, Siragusa R, Halope C. Ultrawideband chipless RFID: Reader technology from SFCW to IR-UWB. IEEE Microwave Magazine. 2019; **20**(6):74-88. DOI: 10.1109/MMM.2019. 2904408

[19] Rezaiesarlak R, Manteghi M. A space–time–frequency anticollision algorithm for identifying chipless RFID tags. IEEE Transactions on Antennas and Propagation. 2014;**62**(3): 1425-1432. DOI: 10.1109/TAP.2013. 2295393

[20] Vena A, Perret E, Tedjini S. High-capacity chipless RFID tag insensitive to the polarization. IEEE Transactions on Antennas and Propagation. 2012; **60**(10):4509-4515. DOI: 10.1109/TAP. 2012.2207347

[21] Rezaiesarlak R, Manteghi M. Chipless RFID: Design Procedure and Detection Techniques. Switzerland: Springer; 2014. ISBN: 978-3319101682

[22] Ramos A, Perret E, Rance O, Tedjini S, Lazaro A, Girbau D. Temporal separation detection for chipless depolarizing frequency-coded RFID. IEEE Transactions on Microwave Theory and Techniques. 2016;**64**(7): 2326-2337. DOI: 10.1109/TMTT.2016. 2568180

[23] Shrestha S, Balachandran M, Agarwal M, Phoha VV, Varahramyan K. A chipless RFID sensor system for cyber centric monitoring applications. IEEE Transactions on Microwave Theory and Techniques. 2009;**57**(5):1303-1309. DOI: 10.1109/ TMTT.2009.2017298

[24] Girbau D, Ramos A, Lazaro A, Rima S, Villarino R. Passive wireless temperature sensor based on time-coded UWB chipless RFID tags. IEEE Transactions on Antennas and Propagation. 2012;**60**(11):3623-3632. DOI: 10.1109/TMTT.2012.2213838

[25] Feng Y, Xie L, Chen Q, Zheng L-R. Low-cost printed chipless RFID humidity sensor tag for intelligent packaging. IEEE Sensors Journal. 2015; **15**(6):3201-3208. DOI: 10.1109/JSEN. 2014.2385154

[26] Dey S, Saha JK, Karmakar NC. Smart sensing: Chipless RFID solutions for the internet of everything. IEEE Microwave Magazine. 2015;**16**(10): 26-39. DOI: 10.1109/MMM.2015. 2465711

[27] Lazaro A, Villarino R, Costa F, Genovesi S, Gentile A, Buoncristiani L, et al. Chipless dielectric constant sensor for structural health testing. IEEE Sensors Journal. 2018;**18**(13):5576-5585. DOI: 10.1109/JSEN.2018.2839689

[28] El Matbouly H, Tedjini S, Zannas K, Duroc Y. Chipless sensing system compliant with the standard radio frequency regulations. IEEE Journal of

Radio Frequency Identification. 2019;
3(2):83-90. DOI: 10.1109/JRFID.2019.
2909092

[29] Paret D. Design Constraints for NFC
Devices. London: Wiley-ISTE; 2016.
ISBN: 978-1-84821-884-0

[30] NFC-enabled mobile devices
worldwide 2012–2018 | Statistic.
Available from: https://www.statista.
com/statistics/461494/nfc-enabled-
mobile-devices-worldwide/ [Acccessed:
August 19, 2019]

[31] Want R. Enabling ubiquitous
sensing with RFID. Computer (Long
Beach Calif). 2004;**37**(4):84-86. DOI:
10.1109/MC.2004.1297315

[32] Lazaro A, Villarino R, Girbau D,
Lazaro A, Villarino R, Girbau D. A
survey of NFC sensors based on energy
harvesting for IoT applications. Sensors.
2018;**18**(11):3746. DOI: 10.3390/
s18113746

[33] Wang X, Gaustad G, Babbitt CW,
Bailey C, Ganter MJ, Landi BJ. Economic
and environmental characterization of
an evolving Li-ion battery waste stream.
Journal of Environmental Management.
2014;**135**:126-134. DOI: 10.1016/j.
jenvman.2014.01.021

[34] Marrocco G. Pervasive
electromagnetics: Sensing paradigms by
passive RFID technology. IEEE
Wireless Communications. 2010;**17**(6):
10-17. DOI: 10.1109/MWC.2010.
5675773

[35] Hahnel D, Burgard W, Fox D,
Fishkin K, Philipose M. Mapping and
localization with RFID technology. In:
IEEE International Conference on
Robotics and Automation, 2004
Proceedings ICRA '04. New Orleans:
IEEE; 2004. pp. 1015-1020. DOI:
10.1109/ROBOT.2004.1307283

[36] Yang P, Wu W, Moniri M,
Chibelushi CC. SLAM algorithm for 2D

object trajectory tracking based on RFID
passive tags. In: 2008 IEEE International
Conference on RFID. Las Vegas: IEEE;
2008. pp. 165-172. DOI: 10.1109/
RFID.2008.4519349

[37] Lauridsen M, Nguyen H,
Vejlgaard B, Kovacs IZ, Mogensen P,
Sorensen M. Coverage comparison of
GPRS, NB-IoT, LoRa, and SigFox in a
7800 km^2 area. In: 2017 IEEE 85th
Vehicular Technology Conference (VTC
Spring). Sydney: IEEE; 2017. pp. 1-5.
DOI: 10.1109/VTCSpring.2017.8108182

[38] AN4914 Application note
Automatic Antenna Tuning (AAT) of
ST25R3911B/ST25R391x devices
Introduction. 2017 Available from:
www.st.com [Acccessed: August 19,
2019]

[39] Lee Y. AN710 Antenna Circuit
Design for RFID Applications.
Microchip Tech. Available from: http://
ww1.microchip.com/downloads/en/
appnotes/00710c.pdf [Accessed:
August 19, 2019]

[40] Kim DH, Park YJ. Calculation of the
inductance and AC resistance of planar
rectangular coils. IEE Electronics
Letters. 2016;**52**(15):1321-1323. DOI:
10.1049/el.2016.0696

[41] Boada M, Lazaro A, Villarino R,
Girbau D. Battery-less NFC sensor for
pH monitoring. IEEE Access. 2019;7:
33226-33239. DOI: 10.1109/
ACCESS.2019.2904109

[42] Liu Q, Zhou J, Chen D. NFC
Antenna Assembly. US9941572B2. 2016.
Available from: https://patents.google.
com/patent/US9941572B2/en

[43] Zhu J-Q, Ban Y-L, Sim C-Y-D,
Wu G. NFC antenna with nonuniform
meandering line and partial coverage
ferrite sheet for metal cover smartphone
applications. IEEE Transactions on
Antennas and Propagation. 2017;**65**(6):

2827-2835. DOI: 10.1109/TAP.2017.
2690532

[44] Gebhart M, Neubauer R, Stark M, Warnez D. Design of 13.56 MHz smartcard stickers with ferrite for payment and authentication. In: 2011 Third International Workshop on Near Field Communication. IEEE; 2011. pp. 59-64. DOI: 10.1109/ NFC.2011.14

[45] Gebhart M, Bruckbaue J, Gossar M. Chip impedance characterization for contactless proximity personal cards. In: 2010 7th International Symposium on Communication Systems, Networks & Digital Signal Processing (CSNDSP 2010), Newcastle upon Tyne. IEEE; 2010. pp. 826-830. Available from: https://ieeexplore.ieee.org/abstract/doc ument/5580309/

[46] Agbinya JI. Wireless Power Transfer. 2nd ed. Denmark: River Publishers; 2015. ISBN: 978-87-93237-62-9

[47] Gvozdenovic N, Mayer LW, Mecklenbräuker CF, Measurement of harmonic distortions and impedance of HF RFID chips. In: The 8th European Conference on Antennas and Propagation (EuCAP 2014); The Hague; 2014. pp. 2940-2944. DOI: 10.1109/EuCAP.2014.6902444/

[48] Couraud B, Deleruyelle T, Kussener E, Vauche R. Real-time impedance characterization method for RFID-type backscatter communication devices. IEEE Transactions on Instrumentation and Measurement. 2018;**67**(8):288-295. DOI: 10.1109/ TIM.2017.2769224

[49] Zhao Y, Smith JR, Sample A. NFC-WISP: A sensing and computationally enhanced near-field RFID platform. In: 2015 IEEE International Conference on RFID (RFID); San Diego: IEEE; 2015. pp. 174-181. DOI: 10.1109/RFID.2015. 7113089

[50] de Oliveira Filho JI, do Prado Villarroel Zurita ME. Development of NFC TAG for temperature sensing of premature newborns in neonatal incubators. In: 2017 2nd International Symposium on Instrumentation Systems, Circuits and Transducers (INSCIT). Fortaleza: IEEE; 2017. pp. 1-4. DOI: 10.1109/INSCIT.2017. 8103519

[51] Lorite GS, Selkälä T, Sipola T, Palenzuela J, Jubete E, Viñuales A, et al. Novel, smart and RFID assisted critical temperature indicator for supply chain monitoring. Journal of Food Engineering. 2017;**193**(1):20-28. DOI: 10.1016/j.jfoodeng.2016.06.016

[52] Vicente JM, Avila-Navarro E, Juan CG, Garcia N, Sabater-Navarro JM. Design of a wearable bio-patch for monitoring patient's temperature. In: 2016 38th Annual International Conference of the IEEE Engineering in Medicine and Biology Society (EMBC); Orlando: IEEE; 2016. pp. 4792-4795. DOI: 10.1109/EMBC.2016.7591799/

[53] Jeong H, Ha T, Kuang I, Shen L, Dai Z, Sun N, et al. NFC-enabled, tattoo-like stretchable biosensor manufactured by "cut-and-paste" method. In: 2017 39th Annual International Conference of the IEEE Engineering in Medicine and Biology Society (EMBC); Seogwipo: IEEE; 2017. pp. 4094-4097. DOI: 10.1109/ EMBC.2017.8037756

[54] Kollegger C, Greiner P, Steffan C, Wiessflecker M, Froehlich H, Kautzsch T, et al. A system-on-chip NFC bicycle tire pressure measurement system. In: 2017 IEEE 60th International Midwest Symposium on Circuits and Systems (MWSCAS). Boston: IEEE; 2017. pp. 60-63. DOI: 10.1109/ MWSCAS.2017.8052860

[55] Boada M, Lazaro A, Villarino R, Girbau D. Battery-less soil moisture measurement system based on a NFC

device with energy harvesting capability. IEEE Sensors Journal. 2018; **18**(13):5541-5549. DOI: 10.1109/ JSEN.2018.2837388

[56] Lazaro A, Boada M, Villarino R, Girbau D. Battery-less smart diaper based on NFC technology. IEEE Sensors Journal. 2019:1-1. DOI: 10.1109/ JSEN.2019.2933289

[57] Azzarelli JM, Mirica KA, Ravnsbæk JB, Swager TM. Wireless gas detection with a smartphone via rf communication. Proceedings of the National Academy of Sciences. 2014; **111**(51):18162-18166. DOI: 10.1073/ pnas.1415403111

[58] Halperin D, Heydt-Benjamin TS, Ransford B, Clark SS, Defend B, Morgan W, et al. Pacemakers and implantable cardiac defibrillators: Software radio attacks and zero-power defenses. In: 2008 IEEE Symposium on Security and Privacy (sp 2008). Oakland: IEEE; 2008. pp. 129-142. DOI: 10.1109/SP.2008.31/

[59] Gollakota S, Hassanieh H, Ransford B, Katabi D, Fu K, Gollakota S, et al. They can hear your heartbeats. In: Proceedings of the ACM SIGCOMM 2011 Conference on SIGCOMM - SIGCOMM '11. New York, USA: ACM Press; 2011. pp. 2-13. DOI: 10.1145/ 2043164.2018438

[60] Rose DP, Ratterman M, Griffin DK, Linlin Hou, Kelley-Loughnane N, Naik RK, et al. System-level design of an RFID sweat electrolyte sensor patch. In: 2014 36th Annual International Conference of the IEEE Engineering in Medicine and Biology Society. Chicago: IEEE; 2014. pp. 4038-4041. DOI: 10.1109/EMBC.2014.6944510

[61] Rahimi R, Brener U, Ochoa M, Ziaie B. Flexible and transparent pH monitoring system with NFC communication for wound monitoring applications. In: Proceedings of the IEEE

International Conference on Micro Electro Mechanical Systems (MEMS). Las Vegas: IEEE; 2017. pp. 125-128. DOI: 10.1109/MEMSYS.2017.7863356

[62] Douthwaite M, Georgiou P. Live demonstration: An NFC based batteryless CMOS ISFET array for real-time pH measurements of bio-fluids. In: 2017 IEEE Sensors. Glasgow: IEEE; 2017. pp. 1-1. DOI: 10.1109/ICSENS.2017. 8234027

[63] Lazaro A, Boada M, Villarino R, Girbau D, Lazaro A, Boada M, et al. Color measurement and analysis of fruit with a battery-less NFC sensor. Sensors. 2019;**19**(7):1741. DOI: 10.3390/ s19071741

[64] Anabtawi N, Freeman S, Ferzli R. A fully implantable, NFC enabled, continuous interstitial glucose monitor. In: 2016 IEEE-EMBS International Conference on Biomedical and Health Informatics (BHI). Las Vegas: IEEE; 2016. pp. 612-615. DOI: 10.1109/ BHI.2016.7455973

[65] DeHennis A, Getzlaff S, Grice D, Mailand M. An NFC-enabled CMOS IC for a wireless fully implantable glucose sensor. IEEE Journal of Biomedical and Health Informatics. 2016;**20**(1):18-28. DOI: 10.1109/JBHI.2015.2475236